

Pumping angular momentum by driven chaotic scattering

T Dittrich and F L Dubeibe

Departamento de Física, Universidad Nacional de Colombia, and
Ceiba – Complejidad, Bogotá D.C., Colombia

E-mail: tdittrich@unal.edu.co

Abstract. Chaotic scattering with an internal degree of freedom and the possibility to generate directed transport of angular momentum is studied in a specific model, a magnetic dipole moving in a periodically modulated magnetic field confined to a compact region in space. We show that this system is an irregular scatterer in large parts of its parameter space. If in addition all spatio-temporal symmetries are broken, directed transport of mass as well as angular momentum occurs. The sensitive parameter dependence of the corresponding currents includes frequent sign reversals. Zeros of either quantity entail the exclusive occurrence of the other and thus give rise in particular to angular-momentum separation without mass transport as a classical analogue of spin-polarized currents.

1. Introduction

During two decades of research on chaotic scattering, internal degrees of freedom have not enjoyed much interest. Yet there are numerous reasons to give them a closer look: An internal freedom may provide the additional dimension required to render a scattering system with a single external degree of freedom chaotic [1, 2, 3, 4]. It may also act as a reservoir that absorbs energy from the external motion and stores it temporarily, thus giving the scattering process a transient inelastic character. Concerning applications, it is obvious that in chemical reactions—one of the paradigms of chaotic scattering [5, 6]—the presence of internal freedoms is indispensable. In mesoscopic physics, in turn, the basic entities are electrons or fermionic quasi-particles: Their spin gives rise to a rich phenomenology beyond point-particle physics and presently receives much attention in the context of spintronics [7, 8, 9].

In electronic and other mesoscopic systems, transport is an issue of vital importance. It has been studied in depth in the framework of adiabatic pumps [10, 11, 12, 13], electron counting [14, 15] and of the Kubo and Büttiker formulae [16, 17, 18]. In spintronics, the practical necessity to provide polarized currents has spurred research on directed spin transport [7, 8, 9]. In a different context, the study of ratchets [19], inspired by the biological phenomenon of motor molecules [20, 21, 22], has revealed general physical conditions and numerous mechanisms for directed transport to occur in systems far from thermal equilibrium. Also here, internal freedoms are almost always involved and participate actively in transport processes [23], e.g., as functional (configurational) degrees of freedom in motor molecules [24, 25] and as internal heat baths.

In this paper we present a case study of chaotic scattering with an internal degree of freedom, intrinsic angular momentum, and consider how it contributes to irregular scattering and how in turn directed transport of this quantity arises from scattering. The subject bears on various of the research lines mentioned above: We shall invoke much of what is known about chaotic scattering, in particular in periodically driven systems [26, 27]. The coupling of a magnetic dipole to an inhomogeneous magnetic field [28] is crucial for our modelling. Also concerning chaotic dynamics in such a configuration we refer to earlier work [29]; in fact, it is the essential ingredient of one of the first models proposed for irregular scattering [30].

In directed transport, we take all the insights into account that concern the importance of binary spatio-temporal symmetries and their breaking [31, 32, 33, 34]. We can here fall back on direct precursor work on chaotic pumps [35]. The definition of spin current is adopted from quantum contexts to define angular-momentum transport in a classical setting. It should be emphasized that we consider a driving that is both strong and fast [26, 27] and thus not amenable to any perturbative and/or adiabatic approximation. In this sense, we are dealing with strongly nonlinear transport phenomena, far off the regime of linear response and in particular of peristaltic pumping [10, 11, 12, 13]. As a consequence, directed transport is achieved already driving the system via a *single* parameter. The crucial rôle of chaos also distinguishes our work

from recent studies of spin ratchets in ballistic electron systems [36, 37, 38]. Preliminary results have been published on a national platform [39].

As our main achievement, we present conclusive evidence that in classical chaotic scattering systems, polarized currents can be generated, i.e., directed transport of angular momentum occurs independently of and even in the absence of mass (charge) transport. We explain this effect in terms of the interplay of asymmetry and the randomizing action of long unstable trajectories, thus corroborating the decisive rôle of chaotic scattering. It is also manifest in the sensitive parameter dependence of mass as well as angular-momentum currents, which allows for a fine tuning of both quantities. In particular, sign reversals are frequent and zeros of one current give rise to the exclusive dominance of the other. In this way, we achieve a “rectification of angular momentum” in the absence of mass transport.

In 2, we construct our model and justify its peculiarities. We discuss details of the dipole-field coupling that have not been considered previously in the context of chaotic scattering. Section 3 is dedicated to irregular scattering as the basic dynamical category of the system. Various diagnostics are presented such as deflection functions, unstable periodic orbits, and time-delay statistics. Our central subject, directed transport, is approached in 4. We define the relevant transport quantities in terms of reflection and transmission coefficients. Numerical evidence is provided for directed mass as well as for angular-momentum transport, and we point out the manifolds in parameter space where pure currents of either kind occur. Section 5 contains a summary and an outlook towards the quantization of our model with the perspective to construct a chaotic spin pump—evidently a major motivation for the present purely classical study.

2. A model for chaotic scattering with intrinsic angular momentum

2.1. Basic setup—coupling internal to external freedoms

In constructing our model, we attempt to satisfy the following requirements, that (i) the system show chaotic scattering at least in parts of its phase space, as a dynamical mechanism for directed transport, (ii) the potential couple the internal to the external degree of freedom and (iii) vanish identically outside a compact scattering region so that numerical simulations can be restricted to a spatial box of finite extension, and (iv) be periodically time dependent in the form of delta kicks in order to facilitate reducing the dynamics to discrete time, that is, a map.

Moreover, previous work on nonlinear transport mechanisms in ratchets and pumps has revealed a fundamental condition for directed currents to occur [31, 32, 33, 34, 35]: an inhomogeneous phase space reflecting the absence of any spatio-temporal symmetry that would give rise to pairs of otherwise identical trajectories carrying the same current in opposite directions. It can be accomplished in particular if the dynamic is mixed (regular coexisting with chaotic motion) and the associated invariant manifolds exhibit some asymmetry. We take these additional criterion into account in setting up the

model.

Specifically, we choose the internal freedom as an intrinsic angular momentum (in the following we shall also refer to it as spin, wherever its classical nature is obvious). In connection with a charge it gives rise to a magnetic dipole moment that couples to an external magnetic field and thus, if the field is not homogeneous, to the spatial motion of the particle. However, we neglect the Lorentz force as concerns the transversal components of the spatial motion. In this respect, we treat the particle as neutral—in fact, neutrons would even provide a more natural physical realization of our model than electrons. Generally, this is justified as a good approximation if the longitudinal velocity is sufficiently small. As an unwanted side effect, with the Lorentz force we also lose the time arrow inherent in the interaction with the magnetic field, as concerns orbital motion. However, it remains effective through the spin dynamics, see 2.3 below.

We can therefore restrict the set of relevant dynamical variables to the longitudinal coordinate x and its conjugate momentum p , as well as the spin vector $\mathbf{s} = (s_x, s_y, s_z)$. In terms of these variables, the Hamiltonian reads

$$H(p, x, \mathbf{s}; t) = \frac{p^2}{2m_0} - \gamma \mathbf{B}(x, t) \cdot \mathbf{s}, \quad (1)$$

where m_0 is the particle's mass and γ the gyromagnetic ratio.

We choose the space and time dependence of the field as

$$\mathbf{B}(x, t) = (0, B_1(x), B_2(x)) \sum_{n=-\infty}^{\infty} \delta(n\tau - t), \quad (2)$$

with

$$B_1(x) = A_1 f(x + a/2), \quad B_2(x) = A_2 f(x - a/2), \quad (3)$$

and an envelope function

$$f(x) = \exp \left[\frac{-1}{(a/2)^2 - x^2} \right] \Theta [a/2 - |x|], \quad (4)$$

as depicted in figure 1a. This function vanishes outside the interval $[-a/2, a/2]$ yet is infinitely often differentiable.

2.2. Equations of motion

In the Hamiltonian (1), the spin \mathbf{s} plays an exceptional rôle in that kinematically it should be treated as an angular momentum, while there is no corresponding kinetic energy term, and a canonically conjugate angle is not defined. For a correct handling of these subtleties, we follow the development in [28] and obtain the equations of motion

$$m_0 \ddot{\mathbf{x}} = \gamma \nabla (\mathbf{B} \cdot \mathbf{s}), \quad \dot{\mathbf{s}} = \gamma \mathbf{s} \times \mathbf{B}. \quad (5)$$

In all that follows, $m_0 = \gamma = \tau = 1$ is understood. An important feature of (5) is that the spin dynamics preserves the form of a Lorentz force and thus breaks time-reversal invariance (TRI).

The field configuration defined in (3,4) implies that within the intervals $[-a, 0]$ and $[0, a]$, the field varies only in magnitude but not in direction. This allows for further simplifications. We identify the y -coordinate with the local field direction, $\mathbf{e}_y \equiv \mathbf{B}/B$, $B \equiv |\mathbf{B}|$, choose spherical coordinates for the spin,

$$s_x = |\mathbf{s}| \sin \theta \sin \varphi, \quad s_y = |\mathbf{s}| \cos \theta, \quad s_z = |\mathbf{s}| \sin \theta \cos \varphi, \quad (6)$$

and denote $s \equiv |\mathbf{s}| = 1$. Then the y -component of the spin, $m \equiv s \cos \theta$, is the angular momentum canonically conjugate to the azimuth φ , while the polar angle θ becomes a constant of motion, so that the spin dynamics reduces to a mere precession, see figure 1b.

$$\ddot{x} = m dB/dx \quad \dot{\varphi} = -B \quad (7)$$

with $m = \text{const.}$ Note that the sense of precession is inverted under time reversal $t \rightarrow -t$ (keeping $B \rightarrow B$), revealing the time arrow inherent in (5).

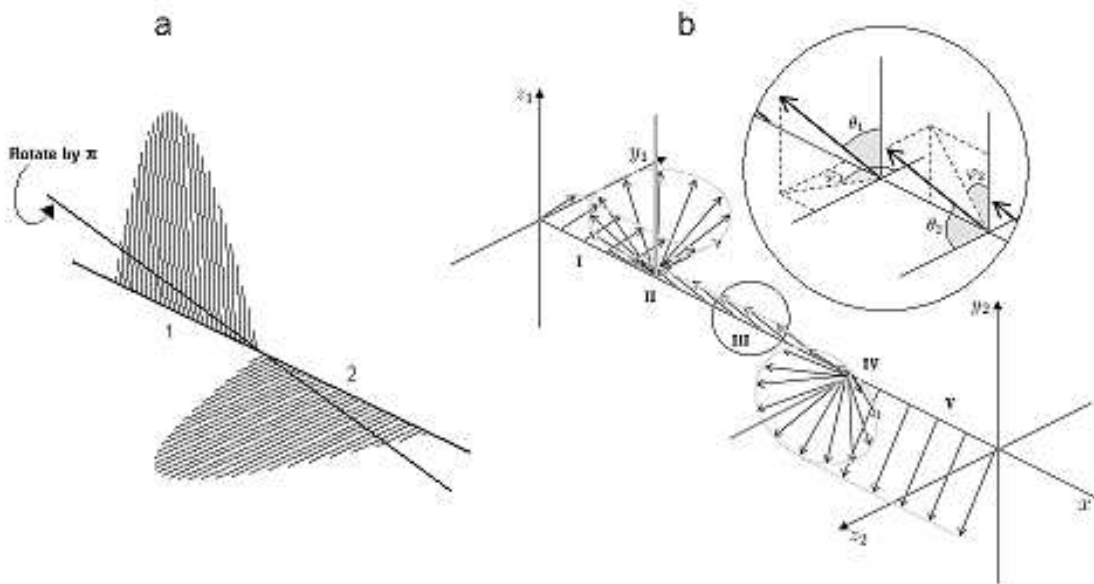


Figure 1. Magnetic field and spin motion in the scattering region. (a) Configuration of the magnetic field (3,4). In each of the two sectors 1 and 2, the field is isotropic, with an angle of $\pi/2$ between the two sectors. For equal amplitudes and identical envelopes, the field is symmetric with respect to rotation by π about the bold line, corresponding to the transformation (9). Rendering the widths and/or the amplitudes of the two field sectors different breaks this symmetry. (b) Schematic representation of the scattering process involving the spin vector \mathbf{s} (bold arrows). In the incoming and outgoing asymptotic regions (phases I, V, resp.) \mathbf{s} remains constant. Within the field sectors 1 and 2 (phases II and IV, resp.) it precesses around \mathbf{B} . Upon passing from sector 1 to 2 (phase III), the angles θ , φ defining the orientation of \mathbf{s} undergo a passive transformation, cf. (8), as depicted in the enlargement (inset).

2.3. Symmetry considerations

For an inhomogeneous but unidirectional magnetic field, according to (7), the projection of the spin onto the field direction is a cyclic variable. This kind of dynamics therefore may give rise to chaotic spatial motion, but will not affect the spin. In order to induce “spin flips” (again abusing quantum terminology), we add a second interaction sector where the field is perpendicular to that in the first, as specified in (3) (see figure 1a). Upon passing from region 1 to 2 or back, the spherical coordinates (6) defining the spin orientation in the two respective systems of reference aligned with the field direction in either region undergo a passive transformation as follows, cf. the inset in figure 1b,

$$\begin{aligned}\theta_2 &= \arccos(\sin \theta_1 \cos \varphi_1), & \theta_1 &= \arccos(\sin \theta_2 \sin \varphi_2), \\ \varphi_2 &= \arctan(\cot \theta_1 \csc \varphi_1), & \varphi_1 &= \arctan(\tan \theta_2 \cos \varphi_2).\end{aligned}\tag{8}$$

If the widths and amplitudes of the two field sections are identical, however, a spatial symmetry remains, namely rotation about the line through the origin and diagonal between the two field directions, see figure 1a. In Cartesian coordinates, it corresponds to the operation

$$x' = -x, \quad y' = z, \quad z' = y.\tag{9}$$

This symmetry would impede directed transport. In order to break it, we choose the two amplitudes distinct, $A_1 \neq A_2$, which gives the difference $A_2 - A_1$ the meaning of a symmetry-breaking parameter.

Besides spatial symmetries, time-reversal invariance deserves some special consideration. As discussed in [31, 32, 33, 34], it must also be broken to achieve directed transport because otherwise the existence of pairs of symmetry-related but counterpropagating trajectories leads to an exact cancellation of currents. In [31, 32, 33, 34, 35], this has been achieved by imposing an asymmetric profile on the driving force. In our case, the driving is symmetric under time reversal, while TRI is lifted by the presence of a magnetic field. This effect, however, is not obtained through the Lorentz force—which indeed we neglect, cf. 2.1. Rather, it is the spin dynamics $\dot{\mathbf{s}} = \gamma \mathbf{s} \times \mathbf{B}$, cf. (5), that is altered under $t \rightarrow -t$.

2.4. Discrete-time dynamics

The impulsive driving allows us to integrate the equations of motion from one kick to the next. Placing time sections immediately before each kick, i.e., $t_n = n\tau - 0^+$, we arrive at the following stroboscopic maps for the two respective field regions

$$p_{n+1} = p_n - 2x_{i,n}B_i(x_{i,n}) \cos \theta_{i,n}/[(a/2)^2 - x_{i,n}^2]^2,\tag{10a}$$

$$\varphi_{i,n+1} = \varphi_{i,n} - B_i(x_{i,n}),\tag{10b}$$

$$x_{i,n+1} = x_{i,n} + p_{n+1},\tag{10c}$$

where $i = 1, 2$, $B_i(x)$ refers to (3), $\varphi_{i,n}$ refers to the frames related by (8), and $x_{i,n} = x_n - (-)^i a/2$. One readily checks that these maps are canonical, that is, the determinant of their stability matrix equals unity.

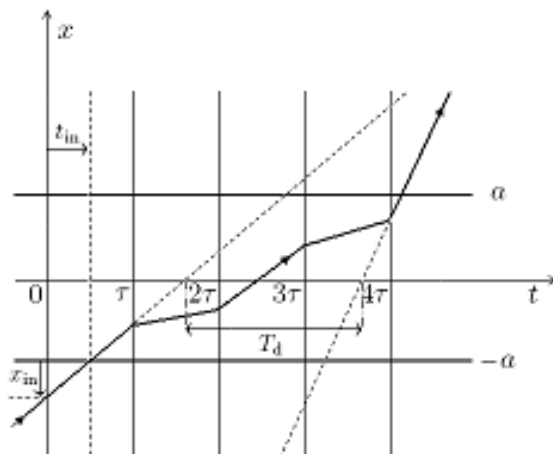


Figure 2. The time lag t_{in} of a scattering trajectory (bold zigzag curve) relative to the periodic kicks of the driving (vertical lines) is defined with respect to the moment when it enters the scattering region at $x = \pm a$. It can alternatively be scaled as a phase shift $\phi_{\text{in}} = 2\pi t_{\text{in}}/\tau$ or a spatial offset $x_{\text{in}} = p_{\text{in}}t_{\text{in}}$. By contrast, the definition of the delay time T_d refers to the extrapolation of the incoming and outgoing asymptotes (dotted lines) forward and backward, resp., till they intersect the line $x = 0$. See text for details.

In this periodically driven scattering system, the phase shift of an incoming trajectory relative to the driving field appears as an additional scattering parameter [26, 27, 35]. It can be defined in various manners; for our particular case of an impulsive driving and a compact spatial support of the field we choose the time lag of the trajectory when it enters the field region at $x = \pm a$ with respect to the most recent kick at $t = n\tau$, cf. figure 2. By definition, its range is $0 \leq t_{\text{in}} < \tau$. Equivalently, it can be rescaled as a spatial shift $x_{\text{in}} = p_{\text{in}}t_{\text{in}}$, $0 \leq x_{\text{in}} < p_{\text{in}}\tau$, or a phase angle $\phi_{\text{in}} = 2\pi t_{\text{in}}/\tau$, $0 \leq \phi_{\text{in}} < 2\pi$.

2.5. Time scales

The dynamics generated by (5) is characterized by three time scales: (i) the temporal separation of the kicks, which defines our unit of time, (ii) the period of spin precession, given by the inverse field strength B^{-1} , and (iii) the typical time to pass the scattering region, of the order of a/p_{in} . As it is our objective to study the participation of the internal freedom in chaotic scattering, we shall work in a regime where all the three time scales are comparable. This prevents, in particular, using adiabatic approximations based on a slow motion of the external coordinate as compared to spin precession.

By contrast, in figure 12b below, we consider the case of fast spin precession $A_i \gg 1$, $i = 1, 2$, in order to anticipate the regime of adiabatic spatial motion typical for experiments with spin- $\frac{1}{2}$ systems.

3. Chaotic scattering

We here consider chaotic scattering as defined by the following properties [40, 41, 42]: (i) the existence of a chaotic repeller consisting of a discrete set of unstable periodic orbits in the scattering region, (ii) rapidly fluctuating deflection functions with self-similar structure, at least in a statistical sense, and singularities accumulating towards the orbits of the chaotic repeller, and (iii) an exponential distribution of delay times inside the scattering region. In the subsequent paragraphs we present numerical evidence that the system devised above complies with all these criteria.

3.1. Deflection functions

In plotting the deflection functions (figure 3) we concentrate on two parameters as incoming variables: the phase ϕ_{in} (left column, panels a,c,e) as an important control parameter in experimental applications and the polar angle θ_{in} (right column, panels b,d,f) as we are interested in the directed transport of angular momentum and ought to make sure that this variable participates in the chaotic scattering.

While these figures show the typical behavior of a chaotic scatterer for large parts of the parameter space, we observe a conspicuously regular pattern in the right column of figure 3 (panels b,d,f) for $\theta_{\text{in}} \gtrsim \pi/2$ that calls for a special explanation. It reflects a strong asymmetry of the scattering process: Trajectories entering region 1 from the left feel a strong repulsive force and bounce back immediately without ever passing into region 2, while trajectories coming in from the right undergo the typical irregular scattering with unbounded delay time. Such long trajectories tend to randomize the outgoing direction and thus lead to approximately balanced transmission and reflection probabilities. We shall see in section 4 that this asymmetry is largely responsible for the transport processes in the system.

3.2. Stable and unstable periodic orbits

From (10a) it is evident that the polar angle θ plays a decisive rôle for the dynamics as its sign determines the local stability of a trajectory. Specifically, upon passing from one field region to the other, the dynamics turns elliptic or hyperbolic according to whether $\cos \theta_{\text{in}}$ is positive or negative, respectively. This is clearly visible also in figure 6b as an absence of peaks for $\theta_{\text{in}} > \pi/2$.

In figure 5 we depict a stable periodic orbit (a) that is inaccessible from outside the scattering region and an unstable one (b) that belongs to the chaotic repeller. They are marked by symbols + and \times , resp., in figure 4a. While for the former, the spin remains at rest, for the latter it exhibits a significant motion that cannot even be reduced to mere precession. In orbital phase space, this orbit forms a double loop, but the corresponding self-crossing is lifted upon taking the spin motion into account.

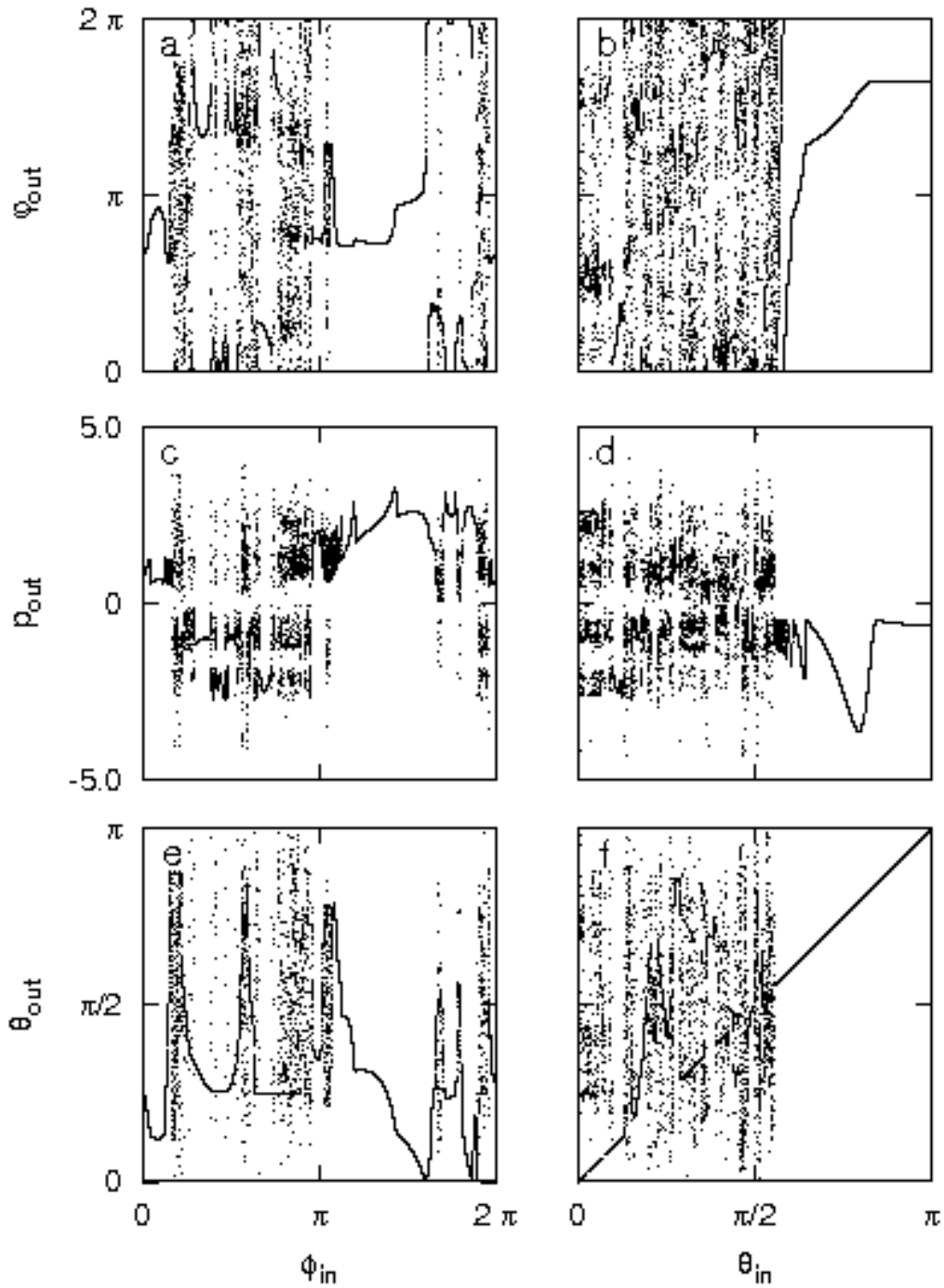


Figure 3. Deflection functions. Outgoing azimuth φ_{out} (a,b), outgoing linear momentum p_{out} (c,d), and outgoing polar angle θ_{out} (e,f) vs. initial phase ϕ_{in} (a,c,e) and vs. initial polar angle θ_{in} (b,d,f), respectively. The other initial conditions and parameters are $p_{in} = 1$, $\theta_{in} = \pi/4$ (a,c,e), $p_{in} = 0.5$, $\phi_{in} = 0$ (b,d,f), and $\varphi_{in} = 0$, $A_1 = 2$, $A_2 = 1$, $a = 4$.

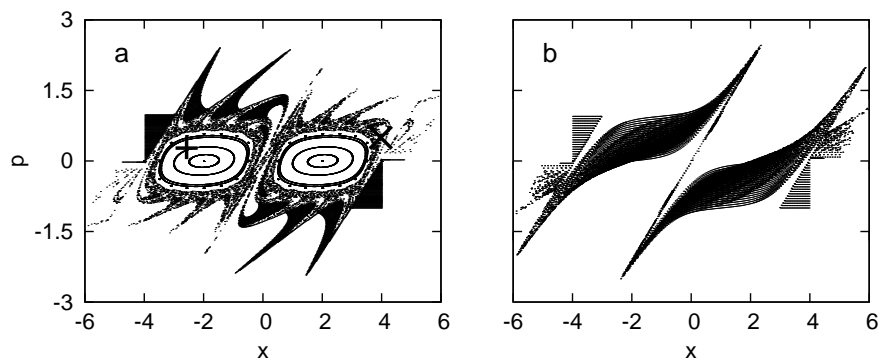


Figure 4. Poincaré sections in the (x, p) -plane for positive (panel a) vs. negative (b) incoming polar angle $\theta_{\text{in}} = -\pi/4$ (b). The other initial conditions and parameters are $\phi_{\text{in}} = 0$, $\varphi_{\text{in}} = 0$, $A_1 = A_2 = 1$ and $a = 4$. The large regular areas in panel a correspond to stable islands not accessible from outside the scattering region. Symbols $+$ and \times indicate periodic orbits depicted in figure 5a,b, resp.

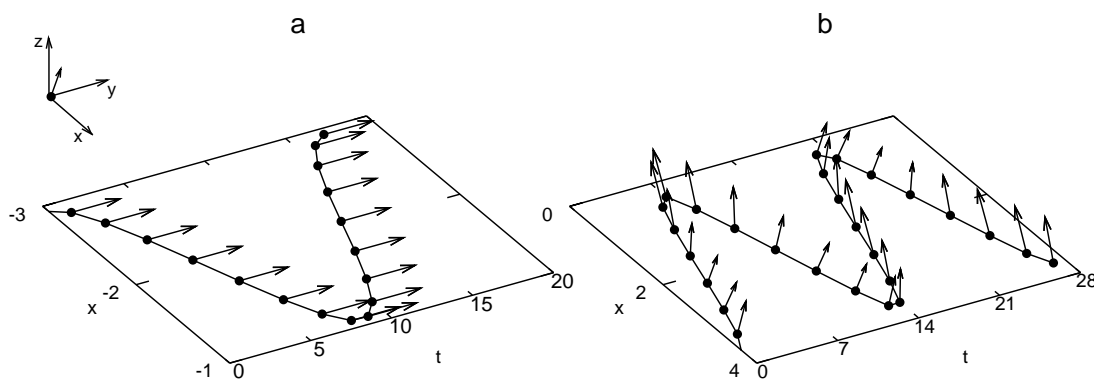


Figure 5. Examples of a stable (a) and an unstable (b) periodic orbit, located respectively in the left stable island in figure 4 (marked by $+$) and the chaotic region (\times). The spatial motion is shown as position x vs. continuous time t , the spin orientation at each t_n in an independent 3-dim. coordinate system moving with the spatial trajectory (inset). While the stable orbit leaves the spin at rest parallel to the field, the unstable one involves a significant spin motion.

3.3. Delay-time statistics

We define the delay time for a given scattering trajectory as usual as the time difference between the incoming and outgoing asymptotes, extrapolated forward and backward, respectively, till the origin, cf. figure 2. This last specification is important as we are dealing with a driven system where in general, energy is not conserved and the outgoing momentum is different from the incoming one.

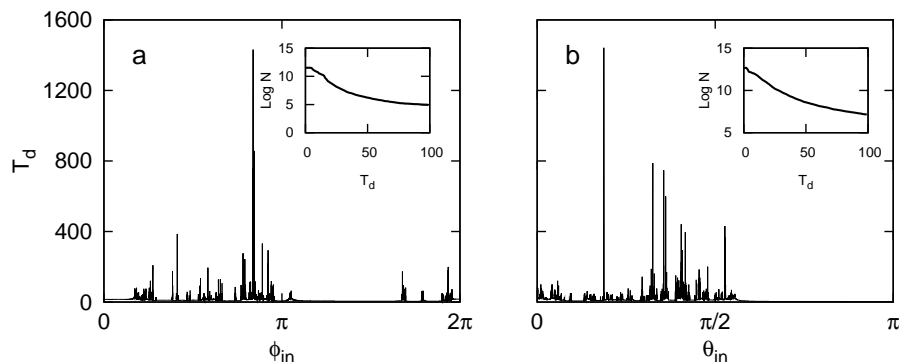


Figure 6. Delay-time statistics as a function of initial phase ϕ_{in} (a) and incoming polar angle θ_{in} (b). The other initial conditions and parameters are $p_{\text{in}} = 1.0$, $\theta_{\text{in}} = \pi/4$ (a), $p_{\text{in}} = 0.5$, $\phi_{\text{in}} = 0$ (b), and $\varphi_{\text{in}} = 0$, $A_1 = 2$, $A_2 = 1$, $a = 4$.

4. Directed transport

We have shown in the preceding sections that our model fulfills the two necessary conditions for directed transport mentioned above, inhomogeneous phase space and absence of binary spatio-temporal symmetries, and therefore expect to find directed currents at least in parts of its parameter space.

4.1. Asymmetric scattering and directed currents

In the context of a scattering system, we define the current as the frequency of particles leaving the scattering region to the right minus the frequency of particles leaving to the left. Denoting $T_{\alpha\beta}$ the fraction of particles transmitted from “channel” α to β and $R_{\alpha\alpha}$ the fraction of particles reflected from α back into α , with $\alpha, \beta = \text{“l”}$ (left) or “r” (right), the current is given by [35]

$$I = (T_{\text{lr}} + R_{\text{rr}} - R_{\text{ll}} - T_{\text{rl}}). \quad (11)$$

In the context of quantum electronics, the spin current is given simply as the difference between the currents in the two spin states “up” vs. “down”, $I_s = I_{\uparrow} - I_{\downarrow}$, with the partial currents defined in turn as in (11). As an immediate generalization to a larger total spin we would write the spin current as a weighted sum of partial currents, with the weights given by the projection of the spin onto some appropriate direction of reference. This suggests to define the spin current in a classical context, where the angular momentum is continuous, as a weighted integral over partial currents parameterized by spherical coordinates,

$$I_s = \frac{1}{4\pi} \int_0^\pi d\theta \sin \theta \int_{-\pi}^\pi d\varphi \cos \theta j(\theta, \varphi), \quad (12)$$

with the current density

$$j(\theta, \varphi) = (j_{\text{lr}}(\theta, \varphi) + j_{\text{rr}}(\theta, \varphi) - j_{\text{ll}}(\theta, \varphi) - j_{\text{rl}}(\theta, \varphi)), \quad (13)$$

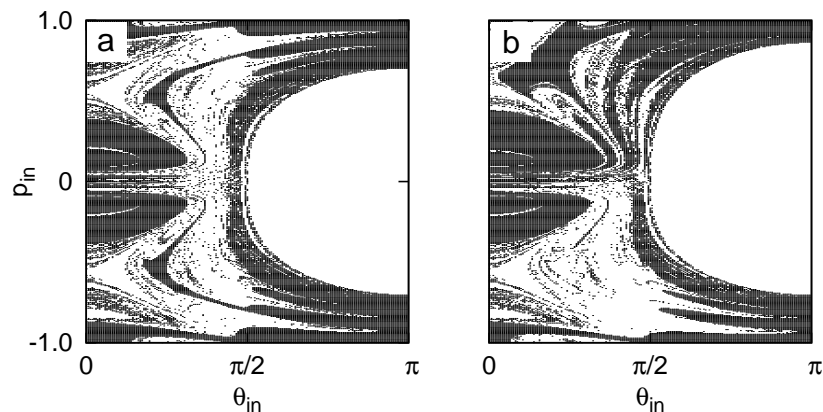


Figure 7. Qualitative outcome of scattering, i.e., transmission (black) vs. reflection (white) as a function of two initial conditions, θ_{in} and p_{in} , for a configuration with (a) and without (b) the spatial symmetry (9). The other initial conditions and parameters are $A_1 = 1$ (a), $A_1 = 2$ (b), and $A_2 = 1$, $a = 4$, $\phi_{\text{in}} = 0$, $\varphi_{\text{in}} = 0$.

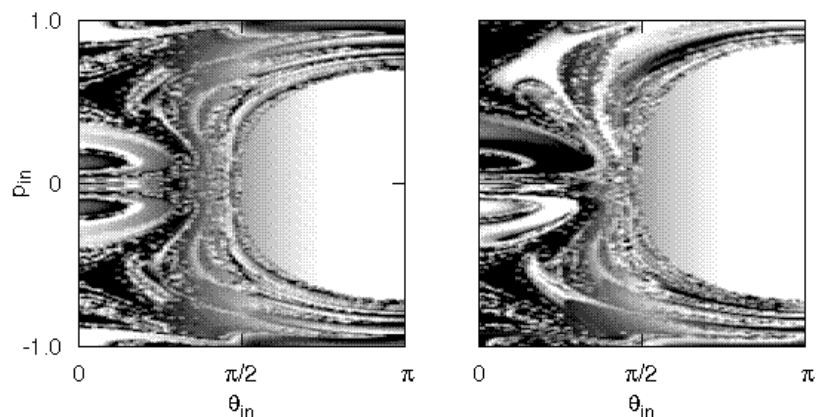


Figure 8. Effective outgoing spin $\cos\theta_{\text{out}}$ (white \equiv negative, grey \equiv zero, black \equiv positive) as a function of incoming polar angle θ_{in} and linear momentum p_{in} , for a configuration with (a) and without (b) the spatial symmetry (9). The other initial conditions and parameters are $A_1 = 1$ (a), $A_1 = 2$ (b), and $A_2 = 1$, $a = 4$, $\phi_{\text{in}} = 0$, $\varphi_{\text{in}} = 0$.

using obvious shorthands for the partial currents between the respective leads. The angles should refer to some suitable laboratory frame, here chosen as the system corresponding to field region 1, cf. (3).

We here assume an initially unpolarized ensemble, corresponding to a homogeneous angular-momentum distribution over the unit sphere. In some cases it is preferable to fix part or all of the initial conditions and to analyze the transport properties as a function of these variables. In figures 7 and 8, we show respectively the outcome of the scattering process, i.e., transmission vs. reflection, and the polarization of the outgoing particles as functions of the initial polar angle and linear momentum. Also in these quantities we observe fractal self-similar structures as in the deflection functions, and

a correspondingly sensitive parameter dependence. The presence (panels a) or absence (panels b) of the symmetry (9) is clearly reflected in the transport features. The large almost void regions that appear in all graphs for $\theta_{\text{in}} > \pi/2$ correspond to trajectories that bounce back immediately after entry, while manifestly asymmetric structures are found only for $\theta_{\text{in}} < \pi/2$. This confirms the mechanism described in 3.1, that chaotic randomization of the outgoing direction occurs only for particles spinning in one sense but not for the other.

The occurrence of directed transport in this system manifestly violates linear-response theory. In terms of static quantities, we are dealing with a non-zero mean (direct) current in the absence of any external mean gradient. Even if we allow for time-dependent input and output, the fact that the system is driven periodically through a single parameter would entail an exact cancellation of transport in a linear-response treatment. The same conclusion results from a Taylor expansion of the current in terms of the driving frequency ω ,

$$I(\omega) = I_0 + I_1\omega + O(\omega^2). \quad (14)$$

If only the I_1 -term were present (linear response), time reversal of the driving $\omega \rightarrow -\omega$ would lead to an exact reversal of the current (“turning the crank backwards pumps in the opposite direction”). In our case, the driving is inherently symmetric in time so that the presence of a directed current is incompatible with linear response [35]. We emphasize that the functional dependence of the current output on the driving amplitude is irrelevant for this conclusion.

The dependence of the polarization on width and amplitude of the field, figure 9a, demonstrates how the spin output could be controlled varying these two parameters that are easily accessible in experiments. The rôle of the symmetry is more directly revealed in figure 9b where the diagonal $A_1 = A_2$ coincides with a zero of the polarization (corresponding to a medium grey shade in the figure). There are, however, other conspicuous zones of vanishing polarization apparently unrelated to this symmetry.

4.2. Angular-momentum transport

The data presented in figures 8 and 9 strongly indicate the existence of polarized currents at least in certain regions of the parameter space. We sketch in figure 10 how a separation of spins could come about in principle in the absence of a net mass current. In order to corroborate its robustness and experimental feasibility, we show in figures 11, 12 global averages both of the particle and the spin current, cf. (11,12). We find zeros of the spin current I_s at appreciable values of the particle current I , corresponding to unpolarized charge transport, as well as zeros of I at high values of I_s . These latter cases amount to a separation of different orientations of angular momentum without net particle transport, that is, to the classical analogue of spin filtering or rectification.

Moreover, in figure 11 we observe a strong dependence of this phenomenon on the breaking of parity, in terms of the ratio A_1/A_2 . As discussed in 2.3 above, it must vanish for $A_1 = A_2$. At the same time, we expect it to diminish in the opposite extreme

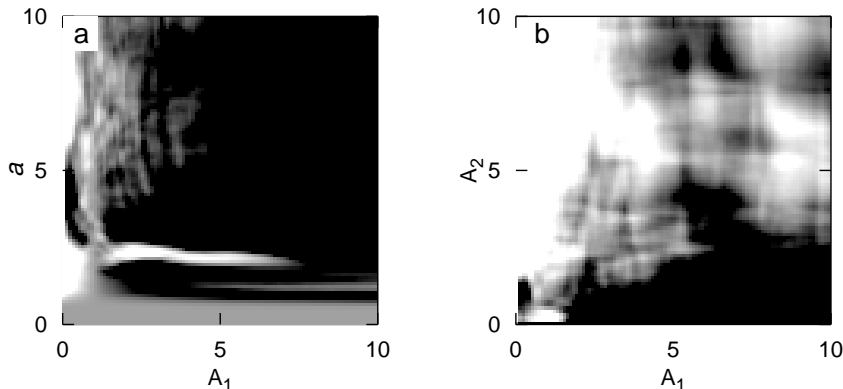


Figure 9. Effective outgoing spin $\cos\theta_{\text{out}}$ (white \equiv negative, grey \equiv zero, black \equiv positive) as a function of width a and amplitude A_1 of the left field sector (a) and of the amplitudes A_1 and A_2 (b), averaged over θ_{in} and p_{in} . The other initial conditions and parameters are $A_2 = 1$ (a), $a = 4$ (b), $\phi_{\text{in}} = 0$ and $\varphi_{\text{in}} = 0$.

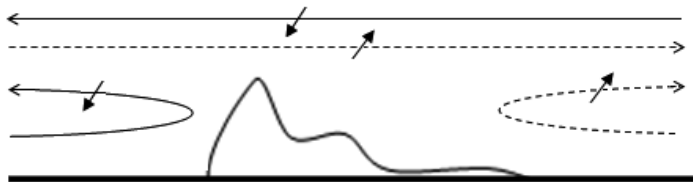


Figure 10. A finite spin current in absence of net mass (charge) transport can arise if particle currents cancel due to parity invariance between transmission and reflection from either side, while the corresponding coefficients for spin scattering lack this symmetry. In this schematic figure, all particles with spin down (full lines) leave to the left, irrespective of the incoming direction, while those with spin up (dotted) all leave towards the right. At the same time, if all currents are assumed to have the same magnitude, mass transport vanishes identically, resulting in pure spin separation.

of $A_1 \ll A_2$ or v.v., as in this limit the effect of the two regions with different field orientation breaking the symmetry (9) is lost. Therefore there should exist an optimum for angular momentum separation at intermediate values of A_1/A_2 .

5. Conclusion

With this work we intend to demonstrate the feasibility of pumping angular momentum in a chaotic scattering system, in the regime of fast and strong driving where adiabatic or perturbative methods would fail. The transport phenomena we observe, both of mass and angular momentum, owe themselves to an interplay of strongly nonlinear dynamics and the breaking of spatio-temporal symmetries. They go far beyond the frame of linear response and do not require a two-parameter driving as in adiabatic pumping. As

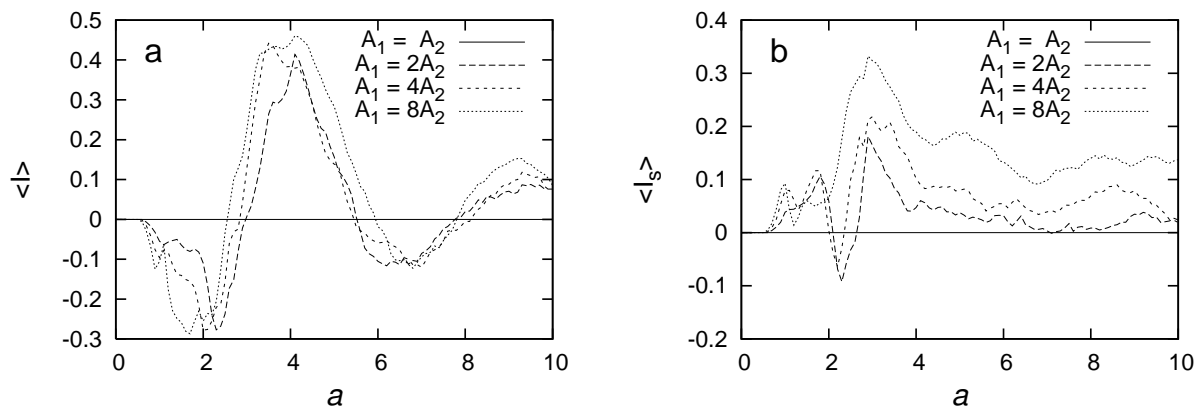


Figure 11. Particle current I (panel a) and spin current I_s (b), averaged over θ_{in} and p_{in} vs. the width of the well a for various values of the ratio A_1/A_2 . Parameters are $A_2 = 1$ and $\varphi_{\text{in}} = 0$.

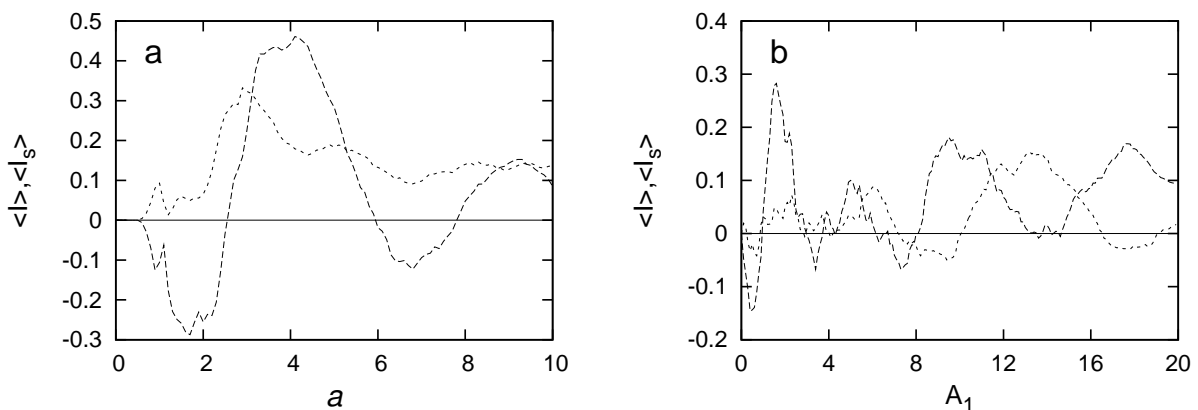


Figure 12. Comparison of particle current I (broken curve) to spin current I_s (dotted), averaged over θ_{in} and p_{in} , as functions of the width a of the scattering region (panel a) and the mean magnetic field strength (panel b). Parameters are $\varphi_{\text{in}} = 0$ and $A_1 = 8$, $A_2 = 1$ (panel a) and $a = 4$, $A_1/A_2 = 1.5$ (b).

a welcome side effect, the sensitive parameter dependence of the scattering process opens the possibility not only to generate angular-momentum currents but also to control them on short time scales and thus to involve them in computation processes.

At the same time, our results constitute an important example of how an internal degree of freedom not only participates in chaotic scattering, but even gives rise to new phenomena. While in this work we focus on transport, the aspect of chaotic scattering with internal freedoms deserves a closer scrutiny in a separate effort.

Another relevant side issue is the fact that spin separation clearly corresponds to a reduction of entropy. In this paper we remain within a perfectly deterministic Hamiltonian setup, a more realistic model including thermodynamic aspects however would urgently have to address this question.

Similarly, connecting the pump on both sides with reservoirs as is usually considered in the context of electronic transport phenomena opens additional possibilities to achieve directed currents. The distributions characterizing the reservoirs (e.g., Fermi distributions parameterized by the chemical potential) require dissipative processes to remain invariant and thus implicitly constitute a time arrow. As a consequence, in such a configuration directed transport can arise even if the scattering system itself does not break time-reversal invariance.

The classical study presented here can be considered as a preparatory survey aiming towards chaotic spin pumping. On grounds of semiclassical arguments, we would expect the mechanisms we elucidate to carry over at least to a “mildly” quantum regime. The electron spin, however, corresponds to the deep quantum limit where among other consequences, the assumption of a slow spin precession, comparable to the other time scales in the system, no longer applies. In order to address this question, we depict in figure 12b mass and spin currents as a function of the magnetic field strength, equivalent to the precession frequency, at constant asymmetry. We see that directed transport does not diminish significantly and we even find instances of pure spin current in a regime where both time scales differ by more than an order of magnitude, giving us some confidence that chaotic pumping of angular momentum could extend down to $s = \hbar/2$.

Acknowledgments

We enjoyed fruitful discussions with F Leyvraz, J Mahecha, K Richter, and C Viviescas. Financial support by Volkswagen Foundation (grant I/78235), Colciencias (grant 1101-05-17608), and Universidad Nacional de Colombia (grant DIB-803940) is gratefully acknowledged. One of us (FLD) thanks for a PhD studentship by Universidad Nacional de Colombia in the program *Becas para Estudiantes Sobresalientes de Posgrado*.

References

- [1] Jung C 1987 *J. Phys. A: Math. Gen.* **20** 1719.
- [2] Jung C 1991 *J. Phys. A: Math. Gen.* **24** 1741.
- [3] Meyer N, Benet L, Lipp C, Trautmann D, Jung C and Seligman T H 1995 *J. Phys. A: Math. Gen.* **28** 2529.
- [4] Papachristou P K, Diakonov F K, Constantoudis V, Schmelcher P, and Benet L, 2004 *Phys. Rev. E* **70** 056215.
- [5] Noid D W, Gray S K, and Rice S A 1986 *J. Chem. Phys.* **84** 2649.
- [6] Gaspard P and Rice S A 1989 *J. Chem. Phys.* **90** 2225.
- [7] Oestreich M 1999 *Nature* **402**, 735.
- [8] Ohno Y, Young D K, Beschoten B, Matsukura F, Ohno H, and Awschalom D D 1999 *Nature* **402** 790.
- [9] Koenig J and Gefen Y 2002 *arXiv: cond-mat/0107450v2*.
- [10] Thouless D J 1983 *Phys. Rev. B* **27** 6083.
- [11] Brouwer P W 1998 *Phys. Rev. B* **58** R10135.
- [12] Altshuler B L and Glazman L I 1999 *Science* **283** 1864.
- [13] Jääskeläinen M, Corvino C, Search C P, and Fessatidis V 2008 *Phys. Rev. B* **77** 155319.

- [14] Kouwenhoven L P, Johnson A T, van der Vaart N C, Harmans C J P M, and Foxon C T 1991 *Phys. Rev. Lett.* **67** 1626.
- [15] Pothier H, Lafarge P, Urbina C, Esteve D, and Harmans M H 1992 *Europhys. Lett.* **17** 249.
- [16] Landauer R 1957 *IBM J. Res. Dev.* **1** 223.
- [17] Büttiker M 1986 *Phys. Rev. B* **33** 3020.
- [18] Büttiker M 1988 *IBM J. Res. Dev.* **32** 317.
- [19] Reimann P 2002 *Phys. Rep.* **361** 57, and refs. therein.
- [20] Spudich J A 1994 *Nature* **372** 515.
- [21] Howard J 2001 *Mechanics of Motor Proteins and the Cytoskeleton* (Sunderland, MA: Sinauer).
- [22] Schliwa M (ed.) 2002 *Molecular Motors* (Wiley-VCH: Weinheim).
- [23] Nakagawa N, Kaneko K 2003 *Phys. Rev. E* **67** R040901.
- [24] Moritsugu K, Miyashita O, and Kidera A 2000 *Phys. Rev. Lett.* **85**, 3970.
- [25] Tournier A L, Smith J C 2003 *Phys. Rev. Lett.* **91**, 208106.
- [26] Henseler M, Dittrich T, and Richter K 2000 *Europhys. Lett.* **49** 289.
- [27] Henseler M, Dittrich T, and Richter K 2001 *Phys. Rev. E* **64** 046218.
- [28] Littlejohn R G and Weigert S 1993 *Phys. Rev. A* **924**, 48.
- [29] Garzón S *Scattering irregular de un spin en un campo magnético gaussiano* 1999 MSc thesis (Bogota: Universidad de los Andes).
- [30] Smilansky U and Blümel R 1989 *Phys. Blätter* **45** 379.
- [31] Flach S, Yevtushenko O, and Zolotaryuk Y 2000 *Phys. Rev. Lett.* **84** 2358.
- [32] Dittrich T, Ketzmerick R, Otto M-F, and Schanz H 2000 *Ann. Phys. (Leipzig)* **9** 755.
- [33] Schanz H, Otto M-F, Ketzmerick R, Dittrich T 2001 *Phys. Rev. Lett.* **87** 070601.
- [34] Schanz H, Dittrich T, and Ketzmerick R 2005 *Phys. Rev. E* **71** 26228.
- [35] Dittrich T, Gutiérrez M, and Sinuco G 2003 *Physica A* **327** 145.
- [36] Scheid M, Wimmer M, Bercieux D, and Richter K 2006 *Phys. stat. sol.* **3** 4235.
- [37] Scheid M, Pfund A, Bercieux D, and Richter K 2007 *Phys. Rev. B* **76** 195303.
- [38] Scheid M, Bercieux D, and Richter K 2007 *N. J. Phys.* **9** 401.
- [39] Dittrich T and Dubeibe F L 2008 *Rev. Col. Fís.* to appear.
- [40] Smilansky U in *Les Houches Lectures XXXVI*, Iooss G, Helleman R H G, and Stora R (eds.) 1981 (Amsterdam: North Holland).
- [41] Ott E (1993) *Chaos* **3** 4.
- [42] Ott E (1993) *Chaos in dynamical systems* 1993 (Cambridge: Cambridge University Press) chap 5.5.